Journal of Pharmaceutical and Biomedical Analysis 78–79 (2013) 105–111

Contents lists available at SciVerse ScienceDirect

Journal of Pharmaceutical and Biomedical Analysis

journal homepage: www.elsevier.com/locate/jpba

Single crystal structure, solid state characterization and dissolution rate of terbinafine hydrochloride

Gislaine Kuminek[a,*], Gabriela Schneider Rauber[a], Manoela Klüppel Riekes[a], Carlos Eduardo Maduro de Campos[b], Gustavo Alberto Monti[c], Adailton João Bortoluzzi[d], Sílvia Lucia Cuffini[a], Simone Gonçalves Cardoso[a]

[a] Programa de Pós-graduação em Farmácia, Universidade Federal de Santa Catarina, Florianópolis, SC, 88040-970, Brazil
[b] Programa de Pós-graduação em Física, Universidade Federal de Santa Catarina, Florianópolis, SC, 88040-970, Brazil
[c] FAMAF – Universidad Nacional de Córdoba & IFEG - CONICET, 5000 Córdoba, Argentina
[d] Depto. de Química, Universidade Federal de Santa Catarina, Florianópolis, SC, 88040-970, Brazil

ARTICLE INFO

Article history:
Received 25 November 2012
Received in revised form 30 January 2013
Accepted 4 February 2013
Available online xxx

Keywords:
Terbinafine hydrochloride
Single crystal structure
Solid state characterization
Intrinsic dissolution rate

ABSTRACT

Terbinafine hydrochloride (TH), a poorly water soluble antifungal agent, was characterized by solid state techniques including differential scanning calorimetry, thermogravimetry, X-ray powder diffraction, optical and electron microscopies, Fourier transform infrared, Raman and solid-state nuclear magnetic resonance spectroscopies and intrinsic dissolution rate (IDR). A colorless single crystal of TH was grown from an ethanol:water solution and its crystalline structure was determined through X-ray single crystal diffraction. Also, a new crystal habit of TH was obtained through the slow solvent evaporation technique revealing a needle-like shape. A comparison between the IDR results for the TH raw material and TH needle-like crystal revealed lower values for the new crystal habit, which can be attributed to the preferential orientation of the crystals in the compressed disks.

1. Introduction

The solid state characterization of active pharmaceutical ingredients (APIs) plays an important role in drug development due to its implications in terms of the physicochemical and biopharmaceutical properties, such as solubility, dissolution rate, bioavailability and stability [1–5]. The characterization and an understanding of solid properties are essential for quality control and regulatory purposes [6,7]. The polymorphism of APIs is routinely controlled since its influence on several solid state properties is a well-established [8]. In some cases, it is also of interest to control the crystal habits and/or morphology of the particles. Recently, researchers in the pharmaceutical industry have demonstrated considerable interest in the possibility of predicting the crystal morphology to optimize drug manufacturing [9]. Regarding the crystal habit, the main differences between solids of different morphologies include the dissolution rate, compaction behavior and powder flow properties [10–12].

The obtainment of distinct crystal habits is greatly influenced by the solvent recrystallization since the morphology is defined by the solute-solvent interaction at various crystal faces [13]. As it occurs with polymorphism, depending on the crystallization conditions (solvent, cooling rate, evaporation rate, final temperature, solution concentration, etc.), several polymorphic forms can be crystallized. The crystal habit or morphology is also dependent on the crystallization conditions. The crystal habit influences the solid state properties, such as fluidity, apparent density, dissolution rate and stability APIs, such as ibuprofen, dipyridamole and phenytoin, which presented distinct morphologies, differ in terms of their physicochemical and/or mechanical properties [13–17].

Terbinafine hydrochloride, (E)-N-(6,6-dimethyl-2-hepten-4-ynyl)-N-methyl-1-naphthalene ethanamine hydrochloride (TH) (Fig. 1), is a potent antifungal agent of the allylamine class. The FDA recommends its use in superficial skin and nail fungal infections since it has a broad spectrum of activity against yeasts, dimorphic fungi and dermatophytes [18–20]. The mechanism of action involves irreversible inhibition of the enzyme squalene epoxidase in fungal ergosterol biosynthesis, promoting intracellular squalene accumulation, which compromises the cell wall integrity [21,22].

This compound is currently marketed in solid state as tablets, capsules and oral granules [18,22] and presents poor solubility in

* Corresponding author. Tel.: +55 48 3721 5066.
E-mail address: giskuminek@gmail.com (G. Kuminek).

0731-7085/$ – see front matter © 2013 Elsevier B.V. All rights reserved.
http://dx.doi.org/10.1016/j.jpba.2013.02.001

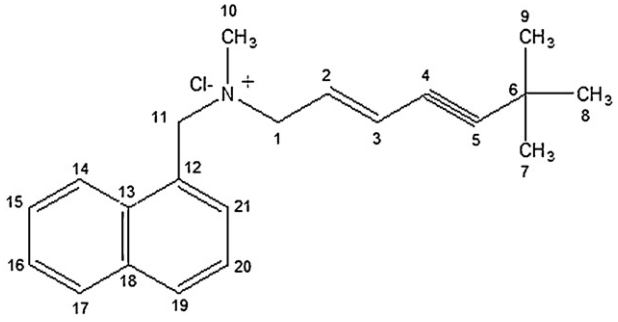

Fig. 1. Chemical structure of TH.

water [23]. However, the data available on the solid state characterization and crystallographic characteristics of TH are incomplete. Detailed searches in the literature and in the Cambridge Structural Database revealed one only crystal structure reported in 2002 by Tedesco, Giron and Pfeffer [24] obtained from synchrotron X-ray powder diffraction data. The authors identified the cell parameters and space group, but no atomic positional coordinates were reported. Furthermore, although polymorphism is a very common phenomenon in APIs, no reports on the polymorphism or solvates of TH appear to have been published in the literature. In some cases, a lack of polymorphism in APIs may be an advantage, since no phase transformations, which could affect the performance of the drug, can occur during manufacturing, storage and administration [25,26]. However, the presence of different TH crystal habits may be of concern and needs to be controlled, since the crystal morphology plays an important role in relation to the technological procedures [27].

Concerning the determination of a new crystal form, structure elucidation based on single crystal analysis is preferred. Essential information, such as iso/anisotropic displacement parameters, disorder locations, atomic coordinates and geometric parameters, is obtained through this approach. Also, single crystal data yields detailed structural information which complements spectroscopic and thermoanalytical analysis and can be useful for quality control, understanding the polymorphism behavior, determining physicochemical correlations and characterizing the morphology.

The aim of this study was to determine the single crystal structure and study the solid properties and dissolution behavior of TH, through an analysis of the commercial raw material (THr) and crystallized samples with different crystalline habits (plate-like crystals [THp] and needle-like crystals [THn]).

2. Materials and methods

2.1. Materials

The TH raw material was obtained from Zhejiang East-Asia Pharmaceutical, batch DC-0107-09122001, and is referred to in this paper as THr. All other materials and solvents used were analytical reagent grade.

2.2. Methods

2.2.1. Obtainment of the crystal-habit-modified TH (THn)

A new crystalline habit of TH was obtained through the slow solvent evaporation technique. A saturated solution of TH in ethyl acetate was maintained at room temperature and protected from light. Under this condition a needle-like crystalline sample was observed, which was characterized through optical microscopy, as reported in Section 2.2.2.5.

2.2.2. Solid state characterization of TH

2.2.2.1. X-ray single crystal diffraction (XRSCD) and X-ray powder diffraction (XRPD). Single crystals of TH were grown from an ethanol:water (50:50 v/v) solution by slow evaporation of the solvent at 281 K. A colorless crystal with a plate-like habit (THp) and dimensions of 0.50 mm × 0.40 mm × 0.13 mm, suitable for XRSCD analysis, was obtained. The crystal was mounted on glass fiber and measurements were taken on a single crystal diffractometer (Enraf-Nonius CAD-4). The radiation used was graphite-monochromated Kα molybdenum radiation (0.71073 Å) and the temperature was set at 293 K. Unit cell dimensions were obtained via least-squares fits of the 2θ values of 25 high-order reflections. The structure was solved by direct methods and refined applying the full-matrix least-squares method using SIR97 [28] and SHELXL97 [29] software programs, respectively. The figure for the molecular structure was produced with the PLATON program [30].

All non-hydrogen atoms were refined with anisotropic displacement parameters. Hydrogen atoms were placed at their idealized positions with distances of 0.93 Å for C—H_{Ar}, 0.97 Å for C—H_2 and 0.96 Å for C—H_3 groups. The U_{iso} values for the hydrogen atoms were fixed at 1.2 times (for aromatic compounds and methylene) and 1.5 times (for methyl) the U_{eq} of the carrier atom (C).

XRPD patterns were collected on a θ–θ X-ray diffractometer (Xpert Pro Multi-Purpose Diffractometer, PANalytical) with Kα copper radiation (λ = 1.5418 Å), operating at a voltage of 45 kV and current of 40 mA, equipped with a sample spinner and a Real Time

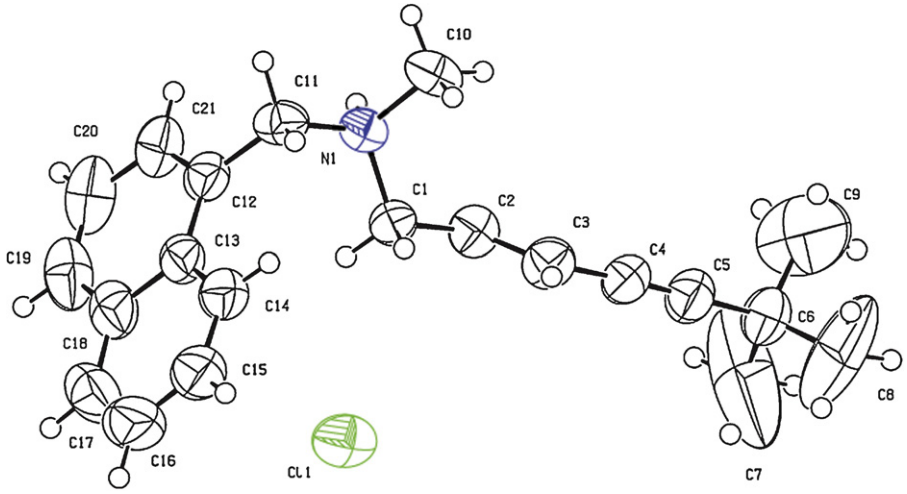

Fig. 2. ORTEP view of the asymmetric unit of TH showing atoms labeling and the 50% probability ellipsoids.

Multiple Strip (RTMS) detector. The measurements were performed at room temperature, scanning from 4° to 50° 2θ using a step size of 0.016° and a step time of 20 s.

2.2.2.2. Differential scanning calorimetry (DSC) and thermogravimetric analysis (TGA). DSC analyses were carried out in triplicate using a Shimadzu calorimeter (DSC-60) with a sensitivity of ±0.1 K, operating in a temperature range of 315–525 K. Samples weighing approximately 1.5 mg were heated in sealed aluminum crucibles (model 201-53090) and scanned at a heating rate of 10 K min^{-1}, under nitrogen air atmosphere (50 mL min^{-1}). The DSC cell was calibrated with indium (mp 429.6 K; ΔH_{fus} = 28.54 J g^{-1}) and zinc (mp 692.6 K).

The mass loss of the samples as a function of temperature was determined in triplicate using a Shimadzu thermobalance (TGA-50). Approximately 3 mg were placed in open platinum crucibles at a heating rate of 10 K min^{-1}, in a temperature range of 303–873 K and under nitrogen atmosphere (50 mL min^{-1}). The instrument was previously calibrated with a standard reference sample of calcium oxalate.

The thermal data obtained were processed using TA60 software.

2.2.2.3. Fourier transform infrared (FTIR) and Raman spectroscopies. FTIR spectra were acquired on a Shimadzu spectrophotometer (FTIR Prestige) at room temperature from 4000 to 400 cm^{-1}. Samples were prepared by mixing 2% (w/w) of the drug in potassium bromide (KBr) and 20 scans were collected at a resolution of 4 cm^{-1}.

The Raman experiments were carried out on a PeakSeeker 785 (RAM–PRO–785) Raman system operating with a diode laser of 785 nm and 300 mW at the source. The Raman radiation collected was dispersed with a grating and focused on a Peltier-cooled charge-coupled device (CCD) allowing a spectral resolution of 6 cm^{-1} to be obtained. The laser was focused on the sample through the 4× objective lens of a microscope giving a focal spot of approximately 2 μm diameter. All spectra were recorded in the spectral window of 200–1800 cm^{-1} with the same acquisition time (30 s). The sample powders were analyzed on glass slides at room temperature.

2.2.2.4. Solid-state nuclear magnetic resonance (SSNMR) spectroscopy. High resolution ^{13}C SSNMR spectra for the API were recorded using the ramp CP/MAS sequence with proton decoupling during acquisition. The solid-state NMR experiments were performed at room temperature on a Bruker Avance II spectrometer operating at 300.13 MHz for protons and equipped with a 4 mm MAS probe. The operating frequency for carbons was 75.46 MHz. Adamantane was used as an external reference for the ^{13}C spectra and to set the Harmann-Hahn matching condition in the cross polarization (CP) experiments. The spinning rate was 10 kHz. The number of transients was set at 384 in order to obtain an adequate signal to noise ratio. The recycling time was 10 s and the contact time during CP was 2 ms. The SPINAL 64 sequence was used for decoupling during acquisition with a proton field H_{1H} satisfying $\omega_{1H}/2\pi = \gamma_H H_{1H}/2\pi$ = 78.2 kHz. A quaternary carbon spectrum was recorded. The spectrum was acquired with the non-quaternary suppression (NQS) sequence, where the ^{1}H and ^{13}C radio-frequency (rf) fields are removed for 60 μs after CP and before the acquisition. This delay allows the carbon magnetization to decay because of the ^{1}H–^{13}C dipolar coupling, resulting in spectra where CH and CH_2 are substantially removed. This experiment thus allows quaternary carbon signals and methyl groups to be identified.

2.2.2.5. Optical microscopy (OM) and scanning electron microscopy (SEM). SEM was performed using a JEOL JSM-6390LV variable-pressure field emission scanning electron microscope (resolution: 3 nm at 30 kV; accelerating voltage: 5 kV; specimen stage: 300 mm by 330 mm (Compucentric); detector: secondary electron). Samples were mounted onto aluminum stubs and sputter-coated with gold under vacuum prior to analysis.

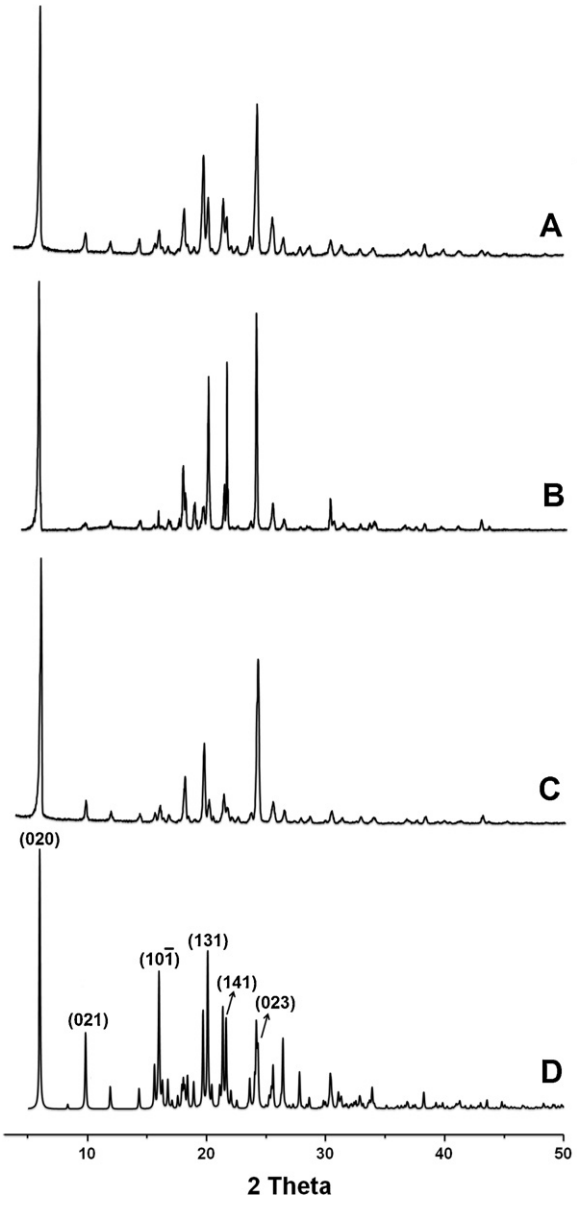

Fig. 3. Diffractograms for TH raw material (A), THn (B) and THp (C) and calculated TH XRPD pattern (D).

OM photographs were taken using a Carl Zeiss Axiophotomicroscope fitted with a HB050 illuminator (Carl Zeiss, Thornwood, NY) at a magnification of 10×. Images were captured with a Zeiss Axiocam digital camera.

2.2.2.6. Intrinsic dissolution rate (IDR). The IDR of TH was evaluated in triplicate using a rotating disk on a Varian dissolution apparatus (VK 7000) according to the specifications of USP [31]. Approximately 100 mg of the drug was compressed in a hydraulic press (ASTA) at 12,000 psi for 1 min in a die of 8 mm diameter disks (surface area 0.5 cm^2)[31]. The apparatus with the compressed disk was firstly maintained in an oven at 40 °C for 15 min. The samples were then rotated at 75 rpm in 250 mL of previously-deaerated 0.001 M HCl (pH 3.0) maintained at 310 ± 0.5 K. Aliquots of 4 mL were withdrawn (with immediate replacement) at predetermined time intervals (5, 10, 15, 20, 30, 40, 50 and 60 min) and filtered through

Table 1
Crystallographic parameters of TH.

Empirical formula	C_{21} H_{26} Cl N
Molecular weight	327.88
Crystal system	Monoclinic
Space group	$P\,2_1/n$
a (Å)	5.9208(6)
b (Å)	29.420(2)
c (Å)	11.4347(14)
β (°)	97.870(9)
V (Å^3)	1973.0(3)
Z	4
D_{calc} (g cm^{-3})	1.104
Absorption coefficient (mm^{-1})	0.194
F(0 0 0)	704
Crystal size (mm)	0.50 × 0.40 × 0.13
Color	Colorless
Temperature (K)	293(2)
Radiation, λ (Å)	Mo Kα, 0.71073
Measured reflections	3814
Independent reflections	3636 (R_{int} = 0.0275)
Refined parameters	216
Goodness-of-fit on F^2	1.056
Final R indices [$I > 2\sigma(I)$]	R_1 = 0.0655 wR_2 = 0.1734
R indices (all data)	R_1 = 0.1748 wR_2 = 0.2178

0.22 μm filters before measurements were taken on a UV/VIS spectrophotometer (Varian UV/VIS CARY) at 223 nm. At the end of the IDR determination, the disks were recovered, dried at 313 K and their surfaces were analyzed by XRPD and DSC. These analyses were also performed before the IDR determination procedure. Concomitantly to the development of the IDR method, the solubility of TH was determined in order to assure *sink* conditions during the experiment. An excess of the drug was added to the dissolution medium at a rotation of 150 rpm, at 310 ± 0.5 K, and after an equilibration period of 24 h aliquots were passed through a 0.22 μm filter and assayed by the previously described UV method. The statistical analysis of the data obtained for THn and THr was carried out applying the Student's *t*-test, in which significant results presented a probability of less than 5% ($p \leq 0.05$ with a 95% confidence interval). The statistical evaluation of the results was performed in MS Excel® software.

3. Results and discussion

3.1. Solid state characterization of TH

3.1.1. XRSCD and XRPD

The ORTEP view of the TH asymmetric unit is presented in Fig. 2. This compound crystallizes in the monoclinic system, space group $P2_1/n$. Additional crystallographic data are summarized in Table 1. The torsion angle C21–C12–C11–N1 between the carbon skeleton and naphthalene group of −78.0 (5) demonstrates that they present different orientations. The nitrogen atom is protonated and the chloride is found to be closely interacting through an N–H ...Cl hydrogen bond N1...Cl1 = 2.995 Å (3) and N1–H1...Cl1 = 175 (3)° (Table 2). The anion also interacts with the molecule via CH3...Cl contact, both running along the c axis. In relation to the crystal structure presented by Tedesco, Giron and Pfeffer [24], the cell parameters and space group are identical, but with this technique it was possible to obtain much more precise information regarding the structure, for instance, the iso/anisotropic displacement parameters, atomic coordinates and geometric parameters.

Table 2
Hydrogen bonds for TH (Å and°).

D–H...A	d(D–H)	d(H...A)	d(D...A)	<(DHA)
N(1)-H(1)...Cl(1)[a]	0.97(4)	2.03(4)	2.995(3)	175(3)

Symmetry transformations used to generate equivalent atoms:
[a] $x+1/2, -y+1/2, z+1/2$.

Fig. 3 shows the calculated TH XRPD pattern (A) and the diffractograms for THr (B), THn (C) and THp (D). All patterns contain the same Bragg peaks and the major diffraction peaks appeared at 6.01, 9.84, 16.01, 19.73, 20.23, 21.35, 21.65, 24.27 and 26.39°. According to USP [31] the differentiation between the samples and the reference is established in XRPD if the scattering angles of the strongest reflections obtained from a reference material vary by around ±0.10°, while relative intensities may vary considerably, indicating preferential orientation. On this basis, it is possible to affirm that THr, THp and THn presented the same crystalline structure, although the diffraction patterns showed notable preferred orientation. The hkl indexes related to the most noticeable texturized plans are shown in Fig. 3

3.1.2. DSC and TGA

The DSC curves for THr, THn and THp are shown in Fig. 4. Peaks representing fusion events are observed at around the same temperature for all samples (481.68 K, 483.95 K and 484.41 K for THr, THn and THp, respectively), and the onset and endset temperatures are also similar (Table 3). Differences in the heat of fusion for the samples were observed, suggesting the combined effect of crystallization impurities and crystallinity. These calorimetric results are in agreement with the XRPD data confirming that THr, THn and THp present the same crystalline structure.

The corresponding TGA curves for Thr, THn and THp show a similar thermal decomposition pattern and thus it can be concluded that the different crystalline habits may not influence the thermal characteristic of TH. Also, it is possible to observe that drug decomposition occurs immediately after its melting.

3.1.3. FTIR and Raman spectroscopies

The FTIR and Raman analysis (Fig. 5A and B, respectively) provided additional information regarding the intermolecular interactions within the crystalline structure of TH. The Raman spectra for THr presented the most intense peaks at 513, 720, 841, 1287, 1368, 1442, 1462, 1577 and 1633 cm^{-1}. The FTIR spectra for THr presented characteristic bands at 3039.81, 2968.45, 2447.87, 1631.78, 1514.12, 1469.70, 1415.76, 1361.74, 1261.45, and 958.62 cm^{-1}. The aliphatic C—H deformation bands which appear at 2968.45 cm^{-1} refer to the methyl and methylene groups. On the other hand, the high intensity band at 2447.87 cm^{-1} can be attributed to the amine group. The *t*-butyl group led to two axial deformation bands, observed at 1361.74 and 1415.76 cm^{-1}. The axial asymmetric deformations of aliphatic and aromatic C=C are present at 1631.78 and 1514.12 cm^{-1}, respectively. The intense band at 958.62 cm^{-1} can be attributed to the *trans*-substituted olefin.

3.1.4. Solid-state nuclear magnetic resonance (SSNMR) spectroscopy

The ^{13}C CP/MAS spectrum and the respective NQS spectrum for the TH raw material are shown in Fig. 6, while the carbon assignments and chemical shift values are given in Table 4. As shown in Fig. 6A, the CP/MAS spectrum exhibited sixteen well-resolved signals, indicating that there is only one molecule in the crystalline asymmetric unit, in agreement with the XRSCD results. The TH spectrum was assigned by comparison with the solution spectrum, taking into account the solid-state NQS data and with the aid of chemical shift calculations obtained using commercial programs. The NQS spectrum (Fig. 6B) showed seven signals, two of them (28.3 and 41.4 ppm) corresponding to methyl groups, which are not

Table 3
Thermal and calorimetric properties of THr, THn and THp.

Properties	THr	THn	THTHp
Peak temperature (K ± SD[a])	481.68 ± 0.45	483.95 ± 0.23	484.41 ± 0.11
Onset temperature (K ± SD[a])	477.92 ± 0.20	479.44 ± 0.10	481.17 ± 1.11
Endset temperature (K ± SD[a])	484.74 ± 0.49	487.56 ± 0.60	486.87 ± 0.27
Heat of fusion (J g^{-1} ± SD[a])	92.00 ± 8.10	90.07 ± 8.50	119.82 ± 9.03

[a] Standard deviation

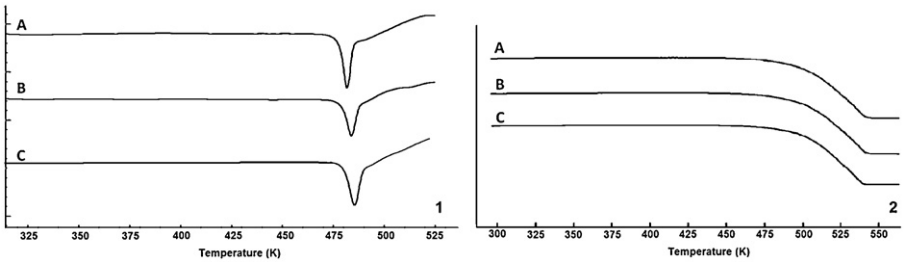

Fig. 4. Thermal data for TH raw material (A) THn (B) THp (C): (1) DSC curves and (2) TGA curves.

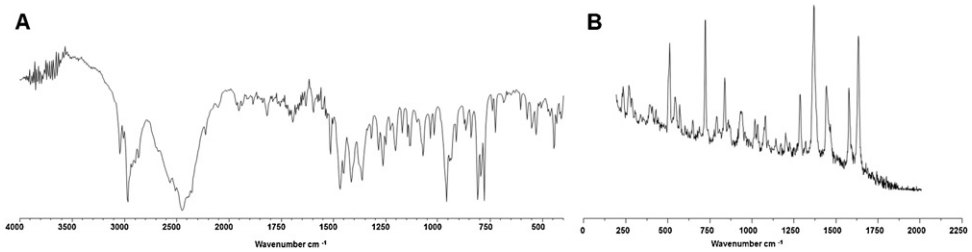

Fig. 5. FT-IR (A) and Raman (B) spectra for TH raw material.

totally suppressed due to rapid methyl group motion. The other five signals relate to the five quaternary carbons in the molecule.

3.1.5. OM and SEM

The images of the TH crystal habits produced from different solvents are represented in The images of the TH crystal habits produced from different solvents are represented in Fig. 7. The THp crystal (Fig. 7A) obtained from a saturated water:ethanol solution (1:1, v/v) showed a plate-like morphology. On the other hand, crystals that were obtained from a saturated ethyl acetate solution (THn) presented a needle-like shape (Fig. 7B). These results indicate that the crystallizing solvent influences the crystal morphology due to the solute–solvent interaction at various crystal–solution interfaces. Changes in the crystal growth kinetics, enhancement or inhibition of growth at certain crystal faces and roundness of the interfaces are some of the factors affected. In addition, the polarity of the solvent and the interaction that leads to its preferential adsorption at selected faces of the solute are critical factors in determining the habit of a crystallizing solid [32,33].

The photomicrographs of THr are shown in Fig. 8 where it can be observed that there is a non-homogeneous particle size distribution and the presence of agglomerates. The analysis of the TH morphology also revealed a plate-like shape, which clearly differed from that observed for THn, which presented a needle-like crystal. It is well known that the crystal morphology plays an important role in pharmaceutical processing and product development, since it influences the physical properties, such as particle orientation, dissolution rate, compaction and compressibility behavior, packing

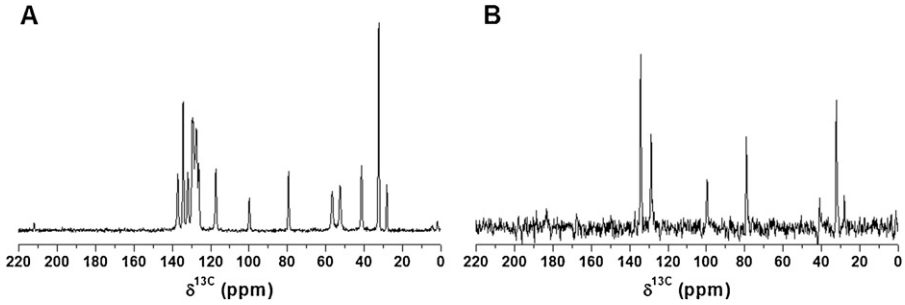

Fig. 6. ^{13}C CP/MAS (A) and the respective NQS (B) spectra for TH raw material.

Table 4
SSNMR data of TH.

Carbon atom	^{13}C NMR chemical shifts
C14-C17, C19-C21	126.2, 127.4, 128.9, 129.6, 131.9
C18	128.8
C12, C13	134.2
C3	117,3
C2	137,59
C4	79,4
C5	99,9
C1, C11	56.7, 52.6
C10	41,4
C7, C8, C9	32,5
C6	28,3

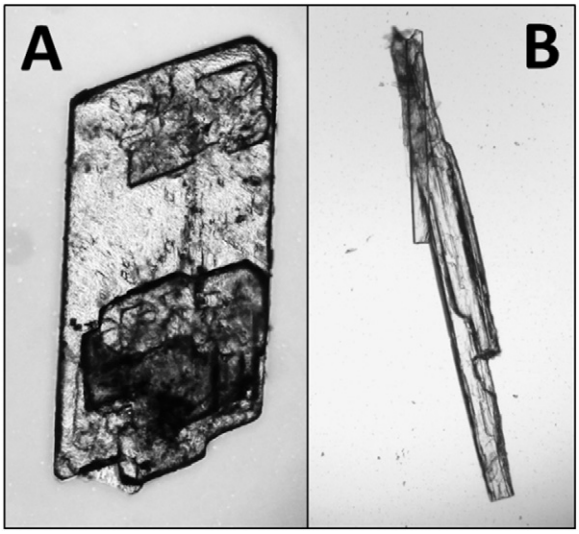

Fig. 7. Images of (A) THp (ethanol:water solution, 1:1 v/v) and (B) THn (ethyl acetate solution).

and powder flow. Therefore, different intrinsic dissolution rates are expected for THr and THn [10–12,34].

3.1.6. Intrinsic dissolution rate (IDR)

Sink condition corresponds to a high capacity of the dissolution medium to dissolve the drug not exceeding 10% of the drug solubility at the end of the test [35]. The maintenance of *sink* conditions during the TH IDR assays was ensured since the drug solubility after an equilibration period of 24 h was 883.42 μg mL^{-1} and the concentration of the drug after 60 min was 62.53 μg mL^{-1}.

Fig. 9 shows the cumulative drug release from solid TH samples in HCl (0.001 M) plotted versus time. The statistical analysis carried out applying the Student's *t*-test revealed that THn and THr

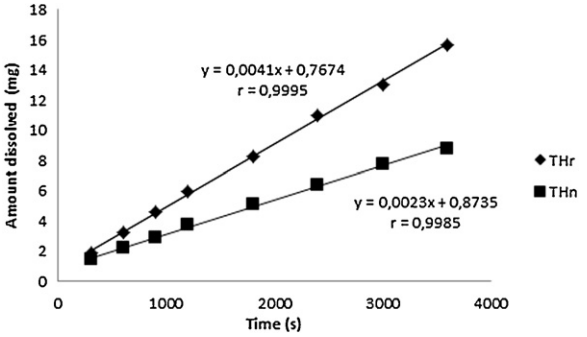

Fig. 9. IDR profiles for (♦) THr and (■) THn.

provided significantly different ($p \leq 0.05$) profiles. The slopes of the straight lines determined by fitting the points of each curve were used to calculate the IDR values, and the results were higher for THr (0.0082 mg cm^{-2} s^{-1}) in comparison to THn (0.0046 mg cm^{-2} s^{-1}). No differences were noted in the results for the DSC and XRPD analyses performed before and after the IDR determination, indicating that there are no pressure or solvent-mediated phase transitions.

It is difficult to rationalize the results directly because there are several processes and sample properties which control the dissolution process, but we can propose the influence of the preferred orientation of the crystals in the compressed disks on the IDR. It is well known that the texturization alters the random distribution of the crystal planes on the surface of a compacted sample, thus differences may occur in the dissolution properties of tablets presenting different degrees of texturization [36]. The exposure of different crystal planes can lead to the interaction of distinct molecular groups with the dissolution medium, which may be associated with differences in the hydrophobicity of the molecule and its wetting capacity. Also, the preferred orientation may influence the ionization degree of weak bases such as TH, since variations in the pH of the boundary layer can occur.

Although the intrinsic dissolution method reduces or even eliminates the effect of particle size and shape, there are several studies suggesting that the preferred orientation of samples affects their dissolution properties [37]. Tenho et al. [38] studied the effect of texture in the determination of the IDR of acetylsalicylic acid and tolbutamide compact disks and their results showed that the most texturized samples clearly had lower IDR values. Also, according to the studies of Prasad et al. [39] on paracetamol single crystals, the crystal face (1 1 0) showed a slightly faster dissolution rate than the face (0 0 1).

Overall, the results obtained in the intrinsic dissolution studies indicate that there are different crystal planes exposed in THn and THr samples, which may influence the dissolution rate of these different crystal habits in the proposed medium. This suggests that the

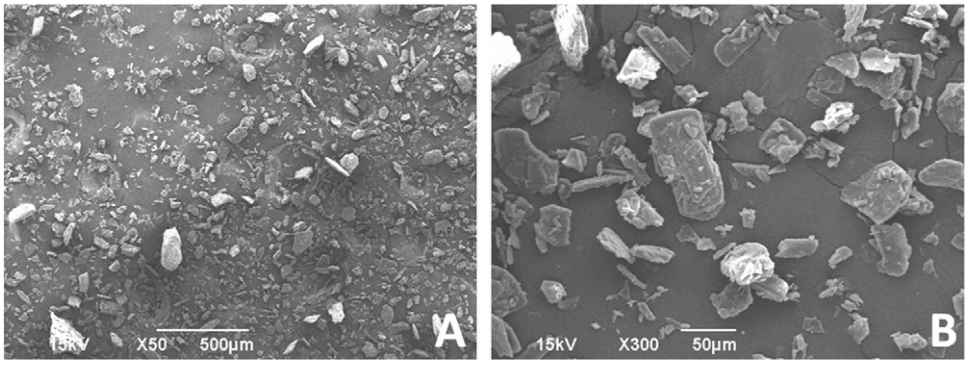

Fig. 8. SEM photographs of TH raw material.

crystalline shape may influence not only the fluidity characteristics of the powder and compression properties but also the dissolution rate, even affecting the drug bioavailability.

4. Supplementary materials

Full tables containing the crystallographic data (except structure factors) have been deposited at the Cambridge Structural Database (CCDC 907850) and these data are available free of charge at www.ccdc.cam.ac.uk.

5. Conclusions

The determination of the single crystal structure and characterization of the solid state of TH were performed. Different crystal habits were obtained and these influenced the TH dissolution rate; however, further studies need to be carried out to evaluate the implications with regard to drug bioavailability. The findings of this research will be useful for studies on the physicochemical control of TH raw materials and highlighted that the control of the crystal habits must be considered as an important factor in preformulation studies and in quality control specifications for these raw materials.

Acknowledgments

The authors would like to thank CNPq, CAPES, FAPESC, CLAF, Fundación Sauberan and CONICET for student fellowships and financial support. Thanks are also due to the Consejo Superior de Investigaciones Científicas (CSIC) in Spain for awarding a license for the use of the Cambridge Structural Database (CSD). XRPD and SEM analyses were carried out at the X-ray Diffraction Laboratory of the Physics Department and Central Electron Microscopy Laboratory, respectively, both at the Federal University of Santa Catarina in Brazil. XRSCD was performed at the Chemistry Department of the same university.

References

[1] L.F. Huang, W.Q. Tong, Adv. Drug Deliv. Rev. 56 (2004) 321–334.
[2] M. Sorrenti, L. Catenacci, G. Bruni, B. Luppi, F. Bigucci, G. Bettinetti, J. Pharm. Biomed. Anal. 63 (2012) 53–61.
[3] S. Agrawal, Y. Ashokraj, P.V. Bharatam, O. Pillai, R. Panchagnula, Eur. J. Pharm. Sci. 22 (2004) 127–144.
[4] J.P. Carini, C. Pavei, A.P.C. Silva, G. Machado, A.S. Mexias, V.P. Pereira, S.L. Fialho, P. Mayorga, Int. J. Pharm. 372 (2009) 17–23.
[5] N. Chieng, T. Rades, J. Aaltonen, J. Pharm. Biomed. Anal. 55 (2011) 618–644.
[6] S.R. Vippagunta, H.G. Brittain, D.J. Grant, Adv. Drug Deliv. Rev. 48 (2001) 3–26.
[7] S. Datta, D.J.W. Grant, Nat. Rev. Drug Discov. 3 (2004) 42–57.
[8] H.G. Brittain, Polymorphism in Pharmaceutical Solids, 2nd ed., Informa Healthcare, New York, 2009.
[9] G. Li Destri, A. Marrazzo, A. Rescifina, F. Punzo, J. Pharm. Sci. 100 (2011) 4896–4906.
[10] N. Rasenack, H. Hartenhauer, B.W. Muller, Int. J. Pharm. 254 (2003) 137–145.
[11] H.A. Garekani, J.L. Ford, M.H. Rubinstein, A.R. Rajabi-Siahboomi, Int. J. Pharm. 208 (2000) 87–99.
[12] A.K. Tiwary, Drug Dev. Ind. Pharm. 27 (2001) 699–709.
[13] P.S. Miroslav Veverka, J. Lokaj, E. Veverkova, Monat. für Chem. 143 (2012) 65–71.
[14] S.R. Byrn, R.R. Pfeiffer, J.G. Stowell, Solid-State Chemistry of Drugs, 2nd ed., SSCI, West Lafayette, IN, 1999.
[15] F.S.H.A. Garekani, A. Badiee, S.A. Mostafa, A.R. Rajabi-Siahboomi, Drug Dev. Ind. Pharm. 27 (2001) 803–809.
[16] A. Nokhodchi, N. Bolourtchian, R. Dinarvand, Int. J. Pharm. 250 (2003) 85–97.
[17] R. Adhiyaman, S.K. Basu, Int. J. Pharm. 321 (2006) 27–34.
[18] A.K. Gupta, N.H. Shear, J. Am. Acad. Dermatol. 37 (1997) 979–988.
[19] G. Petranyi, N.S. Ryder, A. Stutz, Science 224 (1984) 1239–1241.
[20] I. Alberti, Y.N. Kalia, A. Naik, J.D. Bonny, R.H. Guy, J. Control. Release 71 (2001) 319–327.
[21] N.S. Ryder, Br. J. Dermatol. 126 (1992) 2–7.
[22] J.G. Newland, S.M. Abdel-Rahman, Clin. Cosmet. Invest. Dermatol. 2 (2009) 49–63.
[23] The British Pharmacopoeia Stationery Office, London, 2009.
[24] E. Tedesco, D. Giron, S. Pfeffer, Cryst. Eng. Comm. 4 (2002) 393–400.
[25] H.G. Brittain, J. Pharm. Sci. 91 (2002) 1573–1580.
[26] G.G. Zhang, D. Law, E.A. Schmitt, Y. Qiu, Adv. Drug Deliv. Rev. 56 (2004) 371–390.
[27] A.T. Florence, D. Attwood, Physicochemical Principles of Pharmacy, Pharmaceutical, London, 2011.
[28] A. Altomare, M.C. Burla, M. Camalli, G.L. Cascarano, C. Giacovazzo, A. Guagliardi, A.G.G. Moliterni, G. Polidori, R. Spagna, J. Appl. Crystallogr. 32 (1999) 115–119.
[29] G.M. Sheldrick, SHELXL-97. Program for the Refinement of Crystal Structures, University of Göttingen, Göttingen, 1997.
[30] A.L. Spek, Acta Crystallogr. Sect. D 65 (2009) 148–155.
[31] The United States Pharmacopoeia Monographs, 34th ed., National Formulary 29, 2011.
[32] R.J. Davey, Solvent effects in crystallization processes, in: Current Topics in Materials Science, Elsevier, Amsterdam, 1982, pp. 429–479.
[33] Z. Berkovitch-Yellin, J. Am. Chem. Soc. 107 (1985) 8239–8253.
[34] G. Chawla, P. Gupta, R. Thilagavathi, A.K. Chakraborti, A.K. Bansal, Eur. J. Pharm. Sci. 20 (2003) 305–317.
[35] US Pharmacopeial Forum, Pharmacopeial Previews, Rockville, 2004.
[36] M. Tenho, P. Heinanen, V.P. Tanninen, V.P. Lehto, J. Pharmaceut. Biomed. 43 (2007) 1315–1323.
[37] H.M. Burt, A.G. Mitchell, Int. J. Pharm. 5 (1980) 239–251.
[38] J.A. Mikko Tenho, P. Heinanen, L. Peltonenc, V.-P. Lehto, J. Appl. Crystallogr. 40 (2007) 857–864.
[39] K.V. Prasad, R.I. Ristic, D.B. Sheen, J.N. Sherwood, Int. J. Pharm. 238 (2002) 29–41.